Water Research 289 (2026) 124934

Contents lists available at ScienceDirect

Water Research

journal homepage: www.elsevier.com/locate/watres

From fixed points to optimum regions: AI–NSGA-II framework for high-recovery, low-energy brackish water RO

Leili Abkar [a,*], Shima Kamyab [b], Amirreza Aghili Mehrizi [c], Pezhman Abbasi [d], Mark van Loosdrecht [e], Abbas Ghassemi [f], Madjid Mohseni [c]

[a] Department of Process Engineering & Applied Science, Dalhousie University, Halifax, Canada
[b] Department of Electrical and Computer Engineering (ECE), University of Victoria, Victoria, Canada
[c] Department of Chemical and Materials Engineering, Concordia University
[d] Department of Chemical and Biological Engineering, University of British Columbia, Vancouver, Canada
[e] Environmental Biotechnology, Delft University of Technology, Delft, the Netherlands
[f] Department of Civil & Environmental Engineering, University of California, Merced, CA

HIGHLIGHTS

- AI–NSGA-II boosts BWRO recovery from 15 % to 50–70 % with real trade-off maps.
- ANN models validated on real data outperform RSM, predicting EC and *Re* with $R^2 > 0.99$.
- Pareto fronts define optimum regions balancing low energy and high recovery.
- Integrated tuning of flow, pressure, and temperature cuts energy use by over 50 %.
- Optimum regions enable robust BWRO control under seasonal and operating shifts.

GRAPHICAL ABSTRACT

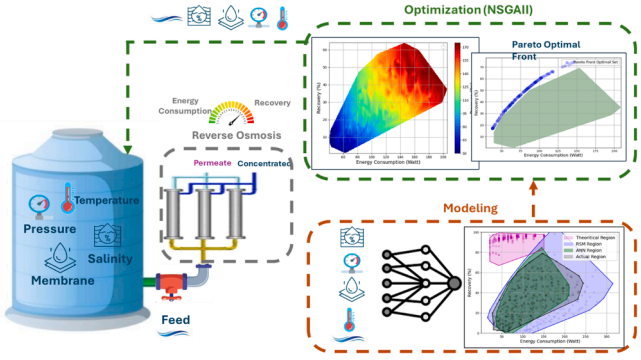

ARTICLE INFO

Keywords:
Energy consumption minimization
Artificial neural networks
Operational factors
Water recovery
Multi-objective optimization
NSGA-II
Sensitivity analysis
Pareto front

ABSTRACT

Escalating global freshwater scarcity demands more energy-efficient and sustainable brackish water reverse osmosis (BWRO) desalination. This study demonstrates how integrating high-fidelity Artificial Neural Network (ANN) surrogates with a robust Non-dominated Sorting Genetic Algorithm II (NSGA-II) can deliver reliable multi-objective optimization for pilot-scale BWRO systems. Unlike conventional polynomial response surface models (RSM), which rely on static assumptions and often oversimplify dynamic membrane processes (and exhibit prediction errors of 15–25 %), the proposed framework directly learns the complex, nonlinear relationships among feed salinity, flow rate, pressure, temperature, and membrane type.

Validated against pilot-scale data with $R^2 > 0.99$ and absolute average relative errors below 5 %, the ANN models accurately predict energy consumption (EC) and recovery (*Re*) under realistic operational conditions. Coupled with NSGA-II, the framework systematically generates Pareto-optimal operating regions that balance low EC (0.6 kWh/m^3) with high *Re* (up to 80 %) while respecting fouling and scaling constraints. This multi-objective approach provides a flexible operating envelope, such as 3–4.5 LPM feed flow and 90–125 psi with

* Corresponding author.
E-mail address: abkar@dal.ca (L. Abkar).

https://doi.org/10.1016/j.watres.2025.124934
Received 15 August 2025; Received in revised form 24 October 2025; Accepted 8 November 2025
Available online 9 November 2025

higher-permeability membranes, surpassing the limitations of single-point optima. The optimized recovery represents a 3- to 5-fold increase over the typical factory baseline (~15 %), translating to energy savings of >50 % and CO_2 emission reductions of 0.1–0.2 kg/m^3. Sensitivity analysis confirms feed flow rate and pressure as dominant drivers of EC (31.3 % and 28.6 % relative factor) and membrane type and flow rate as primary influencers of *Re* (32.2 % and 30.2 %).

This optimum region approach surpasses the limitations of traditional single-point design optimization by providing flexible operating envelopes that accommodate seasonal feed variability, equipment aging, and membrane fouling. All models and the optimization framework are shared via an open-source repository to ensure full reproducibility and facilitate industrial adoption.

Overall, this AI-driven multi-objective optimization framework bridges the gap between theoretical performance and field-ready operation, laying the foundation for more adaptive, cost-effective, and climate-smart brackish water desalination. The modular approach is directly adaptable to multi-stage and hybrid systems, offering a scalable and resilient solution to urgent global water scarcity challenges.

Nomenclature

$\boldsymbol{H}$	Hat value
$\boldsymbol{H}^*$	Warning hat value
$\boldsymbol{N}$	The number of data
$\boldsymbol{Y}$	Predicted response variable
$\boldsymbol{a_i}$	Linear coefficient
$\boldsymbol{a_{ij}}$	Interaction coefficient among the factors
$\boldsymbol{f_o}(\boldsymbol{x})$	Linear transfer function
$\boldsymbol{w_{ij}}$	Weight
μ(X)	Kernel function
$\boldsymbol{\varepsilon}$	Accuracy of the representative function
$\boldsymbol{\sigma}^2$	Variance
$\boldsymbol{\theta^{pred}}$	Predicted output
$\boldsymbol{X}_1$	Feed Flow Rate
$\boldsymbol{X}_3$	Salinity
EC	Energy consumption
R^2	Coefficient of determination
AARE	Absolute average of relative error
RMSE	The root of the mean square error
X	Matrix with a size of ($N \times D$)
X^T	Transpose matrix of X
D	The levels of factors
a_0	Coefficient constant
a_{ii}	Quadratic coefficient
$f_h(x)$	Logistic sigmoid transfer function
b_i	Bias
Z^T	Transported layer of the outputs
$\vartheta_k^*, \vartheta_k$	Slack parameters
y	Tuning factor
θ^{exp}	Experimental output
$x_{v,i}$	The ith data of the input factor
X_2	Temperature
X_4	Pressure
Re	Recovery
RE	Relative error
MSE	Mean square error
RF	Relevancy factor

1. Introduction

Global water scarcity, exacerbated by population growth, climate change, and industrialization, poses significant challenges to water quality and availability (Boretti et al., 2018; DeNicola et al., 2015; Raju et al., 2018). Desalination technologies, particularly reverse osmosis (RO), are critical for producing potable water from brackish and seawater sources (Jones et al., 2019; Shahid and Choi, 2022). However, RO systems, including brackish water reverse osmosis (BWRO), are energy-intensive, consuming approximately 3.7 kWh/m^3 compared to 68–650 kWh/m^3 for thermal desalination methods (Kokabian and Gude, 2019). This high energy demand, coupled with greenhouse gas emissions (0.835–6.1 kg CO_2 eq/m^3), necessitates energy-efficient BWRO systems with high water recovery to enhance sustainability (N. Voutchkov, 2018; Stokes and Horvath, 2009; Skuse et al., 2021). Achieving this requires accurate performance prediction, identification of influential operational parameters, and optimization of trade-offs between energy consumption (EC) and recovery (*Re*).

Traditional models for RO performance prediction, such as mechanistic and semi-empirical mathematical models, rely on simplified assumptions, such as ideal membrane behavior or linear relationships between operational parameters and outcomes (Rall et al., 2020; Brooke et al., 2022). These assumptions limit their accuracy in capturing the complex, nonlinear dynamics of BWRO systems, particularly under varying salinity, pressure, and membrane conditions. For instance, response surface methodology (RSM), a common approach, yields prediction errors of 15–30 % due to its inability to handle high-dimensional, nonlinear data (Abkar et al., 2024). Despite advancements in computational power, these models fail to fully leverage data-driven approaches, leaving gaps in accurately predicting EC and *Re* (Luo et al., 2023; Jawad et al., 2021). Artificial intelligence (AI) methods, such as artificial neural networks (ANN) and least squares support vector machines (LSSVM), excel in modeling complex, nonlinear relationships, offering superior predictive accuracy (Jawad et al., 2021; Ghaedi et al., 2014; Keshtegar et al., 2019; Mijwil, 2018). These methods have been applied to predict flux and *Re* in seawater desalination (Luo et al., 2023; Jawad et al., 2021; Adda et al., 2022), but comprehensive modeling of EC alongside *Re* in BWRO systems, particularly with varying membrane permeabilities, remains underexplored.

Optimization of RO systems is equally critical but faces significant limitations. Many studies focus on single-objective optimization, targeting either EC or *Re* without addressing their trade-offs. For example, (Djebedjian et al., 2008) used genetic algorithms (GAs) to minimize energy use in RO plants, while Ghanbari et al., 2024 prioritized energy in solar/wind/RO designs, and Habieeb et al., 2023 focused on fouling control without multi-criteria analysis (Djebedjian et al., 2008; Ghanbari et al., 2024; Habieeb et al., 2023). Hamza & Shalaby, 2011 similarly optimized for cost and energy efficiency using a single-objective function (Hamza et al., 2011). Nonlinear programming (NLP) approaches (Vince et al., 2008; Lu et al., 2007) often rely on fixed assumptions, limiting adaptability to real-world variability. Moreover, optimization studies often employ traditional algorithms, such as basic heuristic schema or deterministic methods, which lack robust Pareto front handling (e.g., finding optimized regions while facing seasonal salinity

changes). Guria et al., 2005 applied a simple GA for RO optimization, missing elite sorting and diversity preservation, while Behzadi et al., 2022 and Antipova et al., 2013 used basic optimizers for hybrid systems, limiting solution diversity (Guria et al., 2005; Behzadi et al., 2022; Antipova et al., 2013). Additionally, many studies lack sensitivity analyses to identify influential parameters, hindering actionable insights. For instance, Du et al., 2015 and Nazif et al., 2020 optimized RO systems but provided limited factor impact mapping (Du et al., 2015; Nazif et al., 2020). Finally, reproducibility is a significant gap, as few studies share code or data. Al-Obaidi et al., 2019 and Du et al., 2015 developed closed-source models, limiting their N applicability (Du et al., 2015; Al-Obaidi et al., 2019). A detailed comparison of these gaps is provided in Table S1 of the Supplementary Information.

The unique challenges of BWRO further underscore the need for advanced optimization approaches. Unlike seawater reverse osmosis (SWRO), which handles high-salinity feeds (~35,000 ppm), BWRO operates at lower salinities (1000–10,000 ppm), enabling higher recoveries (75–85 %) but increasing scaling risks (e.g., calcium carbonate) (Tong and Elimelech, 2016). BWRO also faces distinct fouling dynamics, with scaling from sparingly soluble salts dominating over SWRO's biofouling and osmotic backpressure, requiring flexible optimization of antiscalant dosing, *Re*, and energy recovery devices (Wilf and Bartels, 2005). Energy recovery devices, critical in SWRO for up to 50 % energy savings, have less impact in BWRO due to lower operating pressures, necessitating careful trade-offs between pumping costs, membrane flux, and *Re* (Stover, 2004). While NSGA-II and other multi-objective evolutionary algorithms (MOEAs) have been applied to SWRO or hybrid systems (Behzadi et al., 2022; Antipova et al., 2013), their use in BWRO remains limited, despite BWRO's unique operational envelope demanding robust multi-objective frameworks. However, most previous RO studies have relied on single-point parametric or polynomial models that fail to capture the dynamic variability of real BWRO operation. This produces overly narrow or idealized optimum settings that do not adapt to seasonal salinity shifts, temperature changes, or membrane aging.

To bridge this gap, this study integrates a multi-output ANN, trained on pilot-scale BWRO data, with the Non-dominated Sorting Genetic Algorithm II (NSGA-II) to develop a multi-objective optimization framework. Unlike single-output ANN models (Mahadeva et al., 2023)or static NLP methods (Vince et al., 2008; Lu et al., 2007), our approach captures nonlinear interactions between EC and *Re*, generating a Pareto-optimal operating region that enables flexible tuning of operational parameters (e.g., feed flow rate, pressure, membrane type) under real-world BWRO conditions, such as salinity variations and membrane fouling.

This framework employs ANN and LSSVM to model EC and *Re*, comparing their predictive accuracy against RSM to validate improvements over traditional models. Further, the study evaluates the influence of operational parameters (salinity, feed flow rate, temperature, pressure) and two membrane types (AK2540TM and AG2540TM) through sensitivity analyses to identify the most influential factors. Unlike prior single-objective studies, this work applies NSGA-II (Nour-Mohammad and Fakhroleslam, 2025; Deb et al., 2002) to explore Pareto-optimal trade-offs, systematically mapping a practical optimum region that balances EC and *Re* under real-world constraints. NSGA-II's elite sorting and crowding distance metrics ensure robust exploration of the solution space, surpassing traditional algorithms. Additionally, all models and data are shared via an open-source repository (https://github.com/s2kamyab/Reverse-Osmosis)to enhance reproducibility and facilitate industrial adoption. Using a comprehensive dataset from a pilot-scale BWRO system, this work seeks to provide actionable, field-ready insights for high-*Re*, low-energy BWRO operation, addressing global water scarcity with practical, data-driven solutions.

2. Material and methods

2.1. BWRO setup and operational conditions

A pilot-scale brackish water reverse osmosis (BWRO) system, detailed in our previous study (Abkar et al., 2024), was used to collect experimental data. The system, configured as a single-stage, single-pass setup with four pressure vessels, was designed to operate under varying conditions relevant to BWRO's unique challenges, such as high *Re* (75–85 %) and scaling risks from sparingly soluble salts (Tong and Elimelech, 2016). Saline water from a feed tank was processed through a centrifugal pump and a media filter to remove coarse particles before entering a high-pressure pump. The pressurized water passed through RO membranes, producing permeate and concentrate streams. Inline sensors monitored operational parameters: salinity (2000, 2500, 3000, 4000 ppm), temperature (30, 40 °C), pressure (50, 75, 100, 125, 150, 175 psi), and feed flow rate (3, 4, 5, 6 LPM). Two low-energy, high-flow membranes (AK2540TM and AG2540TM, General Electric) were used, with characteristics detailed in Table 1. Fig. 1 illustrates the system setup, including pneumatic pressure gates, flowmeters, and EC display.

2.2. Data collection

A dataset of 378 experimental tests was collected to evaluate the impact of salinity, feed flow rate, temperature, pressure, and membrane type on EC and *Re*. The EC, "W", can be expressed by $W_{pump} = \Delta P \times Q_f$, where ΔP is the pressure differential of the water in the entrance of the membrane module and raw water, and Q_f is the volumetric feed flow rate. Tests were conducted in three runs, each repeated thrice, under controlled conditions to ensure reproducibility. The distribution of input and output parameters is summarized in Table 2 and visualized in Fig. 2, demonstrating wide dispersion suitable for ANN and LSSVM modeling. Supplementary Tables S2 provide detailed variable levels for AK2540TM and AG2540TM membranes.

2.3. Applicability domain (AD)

The applicability domain (AD) of the dataset was assessed to ensure model reliability, as described in (Hemmati-Sarapardeh et al., 2018; Zhou et al., 2017). The Leverage method (Rakhimbekova et al., 2020) was used to detect outliers, with results visualized via William's plot (Fig. S1). The warning hat value ($H^* = 0.048$) and standardized residual range ($-3 \leq SR \leq 3$) confirmed no outliers, with EC data more centered around $SR = 0$ compared to *Re*. Detailed AD methodology is provided in SI- S1.1.

2.4. Modelling

This study developed and compared three models—Response Surface Methodology (RSM), Artificial Neural Network (ANN), and Least Squares Support Vector Machine (LSSVM)—to predict EC and *Re*, aligning with the objectives of performance prediction, parameter influence analysis, and optimization.

Table 1
Characteristics of AK2540TM and AG2540TM BWRO membranes (general electric), including permeability, surface area, and rejection rates (Abkar et al., 2024).

Parameter	AG2540TM	AK2540TM
Roughness (Rq nm) ± STDV	54.73±1.30	88.88± 1.70
Thickness (nm)+STDV	49.40± 5.60	50.80± 4.23
Permeability (L m^{-2} h^{-1} bar^{-1})	3.90	4.60
Flux (L min^{-1})	2.70	2.70
Rejection (%)	99	99
Surface area (m^2)	2.60	2.50

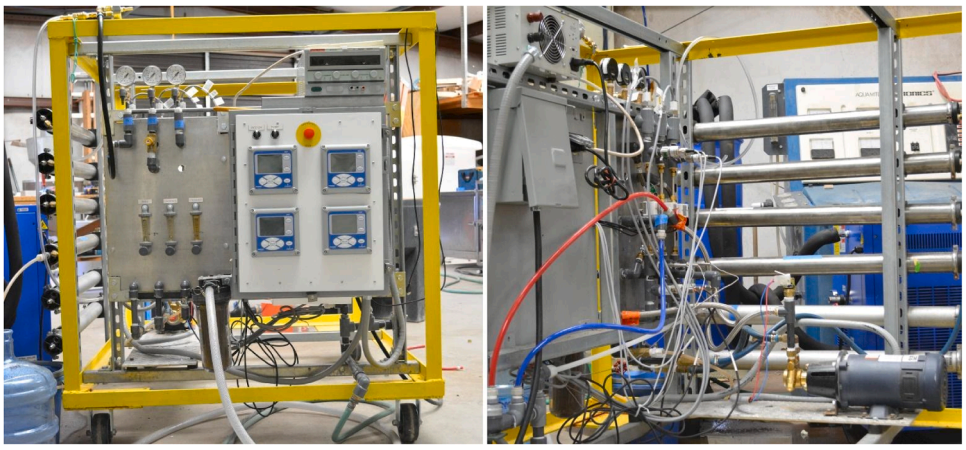

Fig. 1. The pilot-scale BWRO system. The pneumatic pressure gates, flowmeters, and a digital energy consumption display are shown on the left panel. The high-pressure pump and module arrangements are on the right panel.

Table 2
Summary of input (salinity, feed flow rate, temperature, pressure) and output (EC, *Re*) parameter distributions for 378 experimental tests.

Variable	Levels	Values					
Pressure (psi)	6	50	75	100	125	150	175
Feed Flow Rate (L/min)	4	3	4	5	6		
Salinity (ppm)	4	2000	2500	3000	4000		
Temperature (°C)	2	30	40				
Membrane Type	2	BWRO- AG2540	BWRO-AK2540				

2.4.1. Response surface method (RSM)

A randomized optimal response surface methodology (RSM) model was employed, including four independent variables (i.e., input variables): temperature, salinity, feed flow rate, and pressure. Tables S2 and S3 show the independent and dependent variables and their levels in detail for both membranes. The experimental data was fitted by a quadratic Eq. (1) using the Design-Expert Software (DX V.130.0).

$$Y = a_0 + \sum_{i=1}^{n} a_i x_i + \sum_{i=1}^{n} a_{ii} x_i^2 + \sum_{i=1}^{n} \sum_{i=1}^{n} a_{ij} x_i x_j, \; i < j \tag{1}$$

In Eq. (1), Y represents the predicted response variable, a_0, a_i, a_{ii}, and a_{ij} denote the coefficient constant, linear coefficient, quadratic coefficient, and the interaction coefficient among the factors (Salehi et al., 2014). The model's statistical significance was evaluated using Analysis of Variance (ANOVA) at a 95 % confidence interval (Foroughi et al., 2020).

2.4.2. ANN

ANN was employed to capture nonlinear relationships between inputs and outputs, leveraging its ability to model complex systems without predefined experimental designs (Prakash Maran et al., 2013; Talib et al., 2019). ANNs have been effectively employed in various applications, including the performance prediction in seawater and brackish water reverse osmosis (Mahadeva et al., 2023; Chan et al., 2023). The ANN architecture comprises an input layer, hidden layers, and an output layer, all interconnected through the weighted channels forming a multilayer perceptron (Fig. S2).

The input datasets were introduced into the ANN's input layer, and the projected outputs were generated after the processing of the datasets by the activation function in the hidden layers (Mahadeva et al., 2023). Three elements were responsible for the neuron's specialization: the weight derived from the normal distribution, the transfer function, and the bias (i.e., b). Within each neuron, the summation of all weighted input parameters was combined with the b, and the transfer function utilized both these factors to compute the output.

$$f_h(x) = \frac{1}{1 + \exp(-x)} \tag{2}$$

$$f_o(x) = x \tag{3}$$

$$Y = f\left(\sum_{j=1}^{n} w_{ij} x_j + b_i\right) \tag{4}$$

w, b, $f_h(x)$, and $f_o(x)$ in Eqs. (2–4) represented weight, bias, logistic sigmoid, and linear transfer functions. The performance of processes was significantly affected by the number of neurons in the hidden layers (Mehrad et al., 2020). A simple architecture consisting of a single hidden layer (5–32–2), inspired by prior studies on similar desalination datasets (Mahadeva et al., 2023; Wang et al., 2024; Alardhi et al., 2024; Ma et al., 2024) was consider initially. The neurons' number in the hidden layers varied from one to ten, and a trial-and-error approach was employed to determine the optimal number of neurons based on the network's MSE and determination coefficient value (Kardani et al., 2018). To determine the optimal number of neurons in the hidden layers, a grid search was conducted varying neurons from 1 to 10. Fig. S3 shows the Mean Squared Error (MSE) surface for different topologies, confirming that the selected 6 × 8 configuration yields the minimum MSE (1.96×10^{-4}) and maximum R^2 (0.996). The hyperparameters selection and optimization is further explain in S1.5. The learning behavior of the final ANN model is shown in Fig. S4, which illustrates the training and testing MSE over epochs and confirms stable convergence without signs of overfitting. Together, these steps ensure that the ANN architecture robustly captures the nonlinear BWRO relationships while avoiding overfitting. Moreover, to ensure accessibility of technical terminology for readers across engineering disciplines, key terms used in advanced modeling and optimization are defined in a glossary provided in Supplementary Information (SI-Section S1.6).

2.4.3. LSSVM

LSSVM was used for its computational efficiency and high accuracy

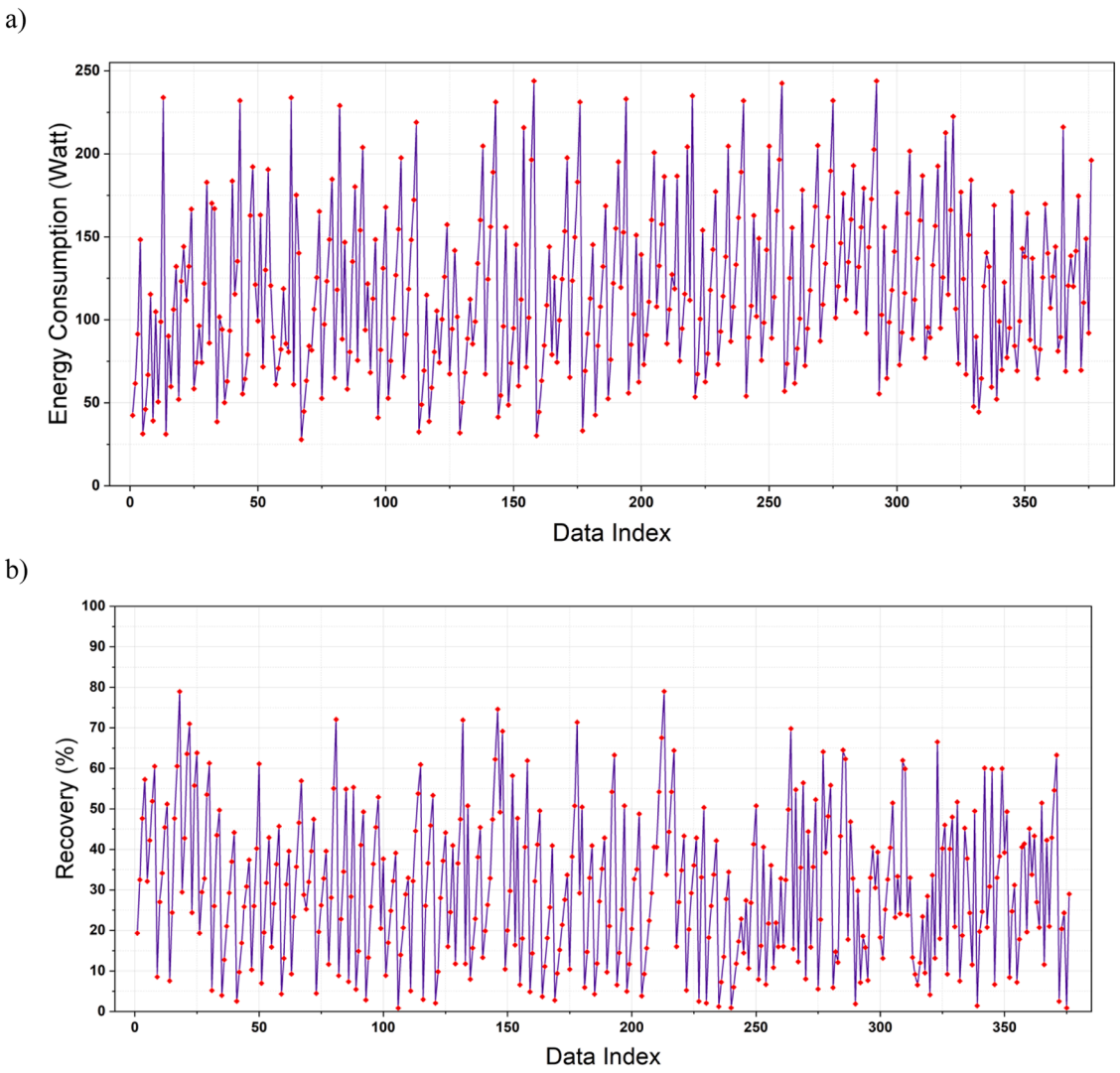

Fig. 2. Distribution of (a) EC and (b) *Re* versus data index for 378 experimental tests, illustrating data dispersion suitable for AI modeling.

in nonlinear regression (Mehrad et al., 2020; Shokrollahi et al., 2015; Zhang et al., 2020; Amer, 2023; Cai et al., 2022; Xue, 2017). While highly effective, its predictive performance depends strongly on selecting optimal hyperparameters (Cai et al., 2022; Xue, 2017). This advantage makes LSSVM particularly suited to modeling nonlinear, high-dimensional datasets compared to other ANN methods (Mehrad et al., 2020; Wu et al., 2020). In this study, a radial basis function (RBF) kernel was selected, with its kernel coefficient, tuning factor (γ), and σ^2 optimized using a population-based crow search algorithm (CSA) (Song et al., 2021; Singh and Ghosh, 2022). The full LSSVM methodology is detailed in SI- Section S1.2 and selection and optimization of hyperparameters explained in S1.5. A schematic of the workflow, including dataset splitting, CSA-based parameter tuning, and testing, is provided in Fig. S5. The final optimized hyperparameters are summarized in Table S4 to ensure reproducibility.

2.4.4. Model significance analysis

Model performance was evaluated using statistical metrics: relative error (RE %), absolute average relative error (AARE %), mean square error (MSE), root mean square error (RMSE), and relevancy factor (RF). These metrics assess prediction accuracy, precision, and parameter influence, enabling comparison of RSM, ANN, and LSSVM models. Calculation methods are provided in SI- Section S1.3.

2.5. Multi-objective optimization, NSGA-II

To identify optimal operating conditions that simultaneously minimize EC and maximize *Re* in the BWRO system, the Non-dominated Sorting Genetic Algorithm II (NSGA-II) was employed. NSGA-II is a widely used evolutionary algorithm for solving multi-objective optimization problems. It operates by evolving a population of candidate solutions toward an optimal trade-off front known as the Pareto front (Deb et al., 2002). The NSGA-II and its pseudocode algorithm (Table S5) to find the pareto optimal set for a set of objectives is fully described in SI-Section S1.4 and S1.5.

NSGA-II was implemented via the Python library "pymoo.algorithms.moo.nsga2.NSGA2." Each individual in the population represents a unique combination of five input parameters relevant to the reverse osmosis process: salinity, pressure, temperature, feed flow rate, and membrane type. The objective functions were defined as $f_1 = EC$ and $f_2 = 1 - Re$, both of which were evaluated using the pre-trained artificial neural network (ANN) model. The neural network employed in this study is a fully connected multilayer perceptron (MLP) designed for regression with five input features. The architecture consists of four layers with the following configuration: an input layer connected to a hidden layer with 32 neurons, followed by a second hidden layer with 64 neurons, a third hidden layer with 32 neurons, and an output layer with two neurons. Each hidden layer uses the ReLU activation function to

introduce non-linearity. NSGA-II parameters, including a population size of 100 individuals and 200 generations, crossover probability of 0.9, and mutation rate of 0.1, are detailed in Table 3a. To reduce the risk of overfitting, dropout layers with a dropout rate of 0.1 were applied after the first two hidden layers. The model was trained using the Adam optimizer over 500 epochs, with learning rate 0.001 a dataset split of 80 % for training and 20 % for testing. This architecture was chosen to balance model capacity with generalization performance, given the relatively limited size of the dataset.

Please note that all the python code for these experiments also exists in our Github repository (https://github.com/s2kamyab/Reverse-Osmosis).

3. Result and discussion

3.1. Sensitivity analysis

Sensitivity analysis was conducted using the relevancy factor (RF, SI-Section S1.3) to identify the influence of input parameters on EC and *Re*. Fig. 3 presents the RF distribution, with values normalized to sum to 100 % for each output.

For *Re*, membrane type was the dominant factor (RF = 32.2 %, $p < 0.01$), attributed to the distinct permeability of AK2540TM (higher permeability, higher flow) versus AG2540TM (lower permeability, lower flow). The membrane characteristics are fully analyzed and discussed in our previous publication (Abkar et al., 2024). Feed flow rate followed closely (RF = 30.2 %, $p < 0.01$), reflecting its direct role in permeate production. Pressure (RF = 17.7 %, $p < 0.01$), temperature (RF = 11.5 %, $p < 0.01$), and salinity (RF = 8.5 %, $p < 0.01$) had lesser impacts, as expected for BWRO's tolerance of low-to-moderate salinity (2000–3000 ppm) (Tong and Elimelech, 2016).

For EC, feed flow rate (RF = 31.3 %, $p < 0.01$) and pressure (RF = 28.6 %, $p < 0.01$) were the primary drivers, as they directly govern high-pressure pump energy, which dominates BWRO energy use (Wilf and Bartels, 2005). Temperature (RF = 18.3 %, $p < 0.01$) and salinity (RF = 17.9 %, $p < 0.01$) showed moderate impact, while membrane type (RF = 20.5 %, $p < 0.01$) had the least influence on consumption due to its indirect effect through permeability differences.

These quantified results highlight operational trade-offs in BWRO systems. High feed flow rates and pressures enhance *Re* but increase EC, underlining the need for optimized operating envelopes to mitigate scaling and fouling risks at higher recoveries (75–85 %) (Tong and Elimelech, 2016). Membrane selection (e.g., AK2540TM for higher *Re*) can optimize performance, particularly in BWRO systems where energy recovery devices have limited impact due to lower operating pressures compared to seawater RO (Stover, 2004). These findings guide operational strategies, such as implementing antiscalant dosing to prevent scaling, and inform subsequent modeling and optimization analyses (Sections 3.2–3.4).

Table 3a
NSGA-II parameter settings for multi-objective optimization, including population size, generations, crossover, and mutation rates.

Parameter	Value	Description
pop_size	100	Population size
Max iteration	500	Number of iterations
Sampling	Real random	Random sampling for initial population
Crossover	SBX (Simulated Binary Crossover)	prob=0.9, eta=15
Mutation	Polynomial Mutation	eta=20, prob=1/n_var
Eliminate_duplicates	True	Removes duplicates individuals
n_offsprings	None (defaults to pop_size)	Number of children per generation
Repair	None	Custom repair operator (not used by default)

3.2. RSM regression

Response Surface Methodology (RSM) models were developed to predict energy consumption (EC) and recovery (*Re*) for AK2540TM and AG2540TM membranes using quadratic polynomial regressions with feed flow rate (X_1), temperature (X_2), salinity (X_3), and pressure (X_4) as predictors (detailed in SI-Section S2.1- Equations 15–18). Tables S6- S9 summarize ANOVA results, with F-values ranging from 247.15 (AK-energy) to 6348 (AG-*Re*) and $p < 0.0001$, confirming statistical significance at a 95 % confidence level.

For AG2540TM, significant terms included linear feed flow rate (coefficient = −8.49 for EC, −7.89 for *Re*, $p < 0.01$) and pressure (coefficient = −0.56 for EC, 0.559 for *Re*, $p < 0.01$), with interaction terms like feed flow rate × pressure (0.12 for EC, −0.03 for *Re*, $p < 0.05$). For AK2540TM, feed flow rate (coefficient = 55.44 for EC, −22.53 for *Re*, $p < 0.01$) and pressure (coefficient = 0.139 for EC, 0.68 for *Re*, $p < 0.01$) were dominant, with significant quadratic terms (e.g., feed flow rate^2: −2.31 for EC, 2.87 for *Re*, $p < 0.05$).

The predicted values from the quadratic models were plotted against experimental values (Fig. 4). The R^2 values for EC AG and AK, and *Re* for AG- and AK were 0.98, 0.89, 0.96, and 0.93, respectively. These R^2 values indicate that Equations 15 and 16 (SI- S2.1) (AG-EC, AG-*Re*) correlated well with experimental data, while Equation 17 (AK-EC, R^2 = 0.89) showed weaker correlation, suggesting limited reliability for EC prediction. Equation 18 (AK-*Re*, R^2 = 0.93) was marginally acceptable.

Relative errors (RE %) were calculated to further evaluate model accuracy, showing differences between predicted and actual datasets: AG-EC (23.34 %), AK-EC (−21.21 %), AG-*Re* (−10.60 %), and AK-*Re* (14.86 %), indicating challenges in accurately predicting EC and *Re*, particularly for AK2540TM. For instance, a 25-psi pressure increase led to a 5–7 % overestimation in EC for AK2540TM, compared to 2–3 % for AG2540TM.

Relative errors (RE %) were calculated to further evaluate model accuracy, showing differences between predicted and actual datasets: AG-EC (23.34 %), AK-EC (−21.21 %), AG-*Re* (−10.60 %), and AK-*Re* (14.86 %). The corresponding absolute average relative errors (AARE %) indicate that the quadratic models have difficulty accurately capturing the true impact of input variables on EC and *Re*, especially for the AK2540TM membrane. For example, while the model structure suggests that increasing operating pressure raises EC, the predicted magnitude can become unstable due to interaction and squared terms, highlighting the risk of overfitting and oversimplification with RSM. These insights confirm that while RSM can approximate general trends, its predictive fidelity for operational setpoints is insufficient for dynamic BWRO conditions. These limitations, driven by BWRO's nonlinear dynamics and variable interactions, highlight the need for AI-based models to better capture complex behaviors.

3.3. ANN and LSSVM

Artificial Neural Network (ANN) and Least Squares Support Vector Machine (LSSVM) models were developed to predict energy consumption (EC) and recovery (*Re*) for the BWRO system, as described in Sections 2.4.2 and 2.4.3. Model performance was evaluated using R-square (R^2), relative error (RE %), absolute average relative error (AARE %), and root mean square error (RMSE) on training and testing datasets (SI-S1.3). Fig. 5 compares predicted vs. actual values for ANN and LSSVM models, showing R^2 values exceeding 0.99 for both EC and *Re*. Specifically, ANN achieved R^2 = 0.997 for EC and 0.996 for *Re*, while LSSVM achieved R^2 = 0.992 for EC and 0.996 for *Re*, indicating superior predictive accuracy compared to RSM models (Section 3.2, R^2 = 0.897–0.986).

To address the influence of data relationships on the ANN's high predictive accuracy ($R^2 > 0.99$, AARE < 5 % for energy consumption, EC, and recovery, *Re*), we compared its performance to linear regression models from our prior work (Abkar et al., 2024; Abkar, 2015) which

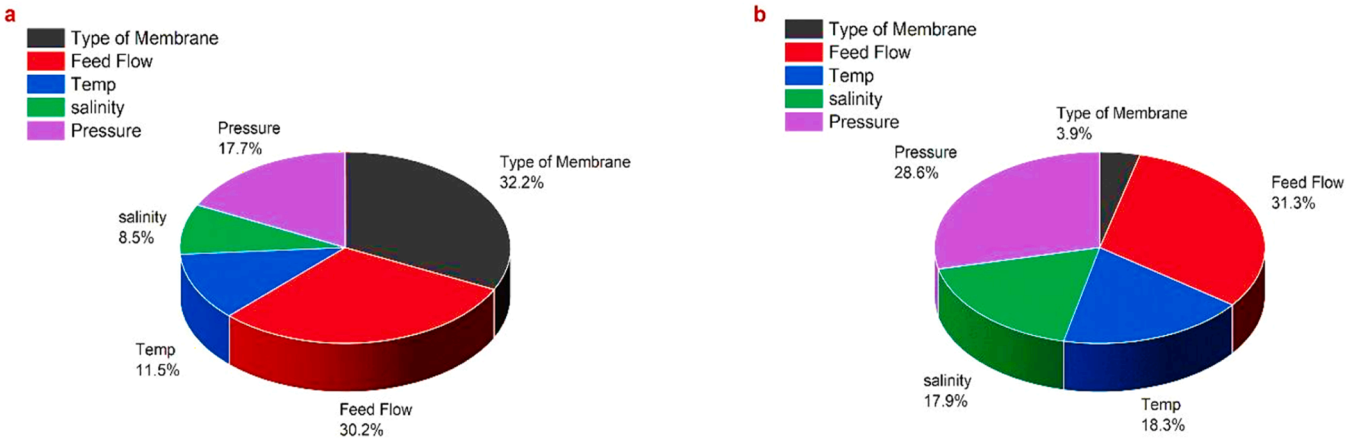

Fig. 3. Relevancy factor (RF) distribution for input parameters (salinity, feed flow rate, temperature, pressure, membrane type) affecting (a) *Re* and (b) EC, showing membrane type (32.2 %) and feed flow rate (30.2 %) as dominant for *Re*, and feed flow rate (31.3 %) and pressure (28.6 %) for EC.

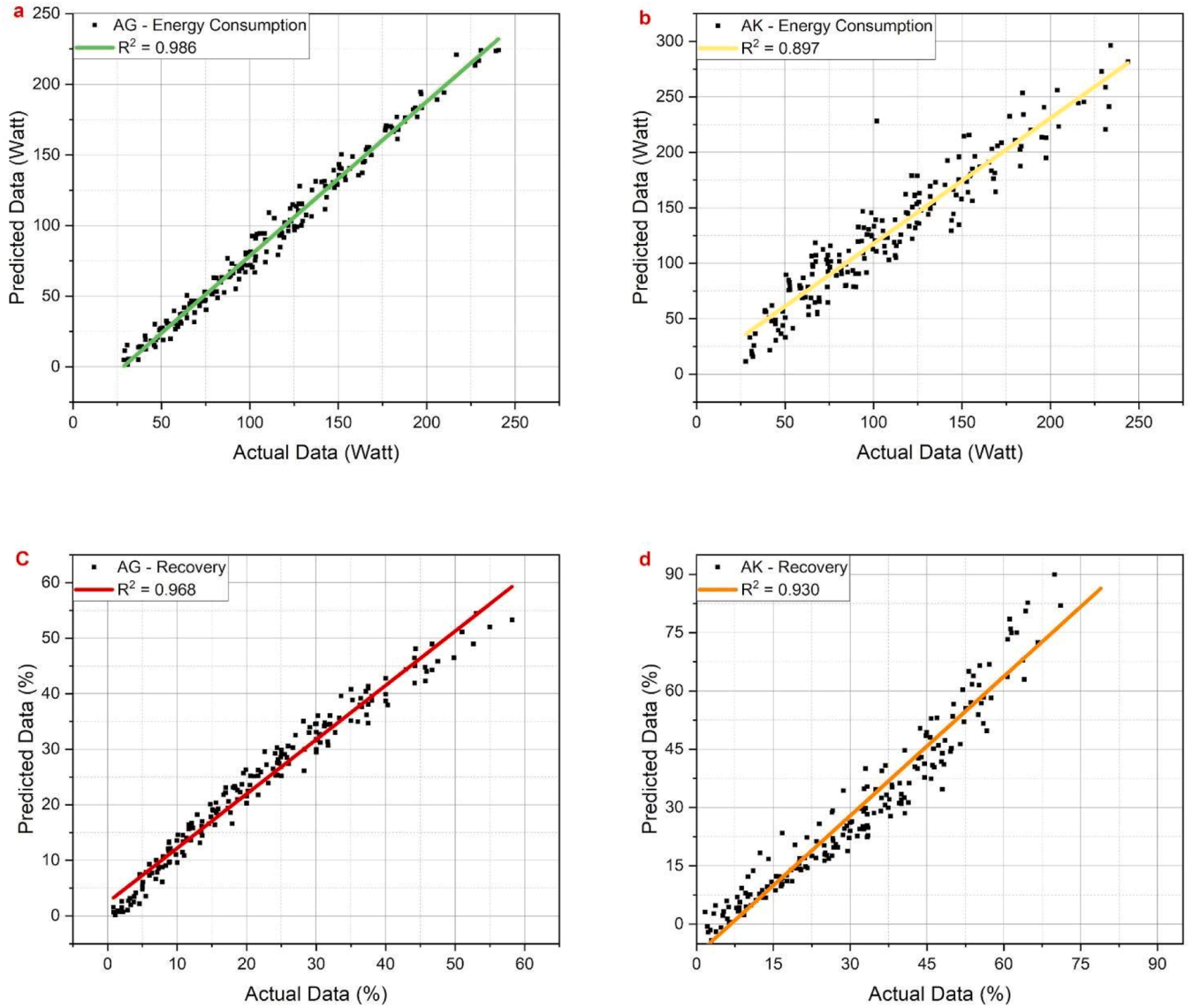

Fig. 4. Predicted values from quadratic equations of EC and *Re* are plotted against the experimental values (a) AG-EC, (b) AK-EC, (c) AG-*Re*, and (d) AK-*Re*. The calculated R^2 values vary between 0.93- 0.986.

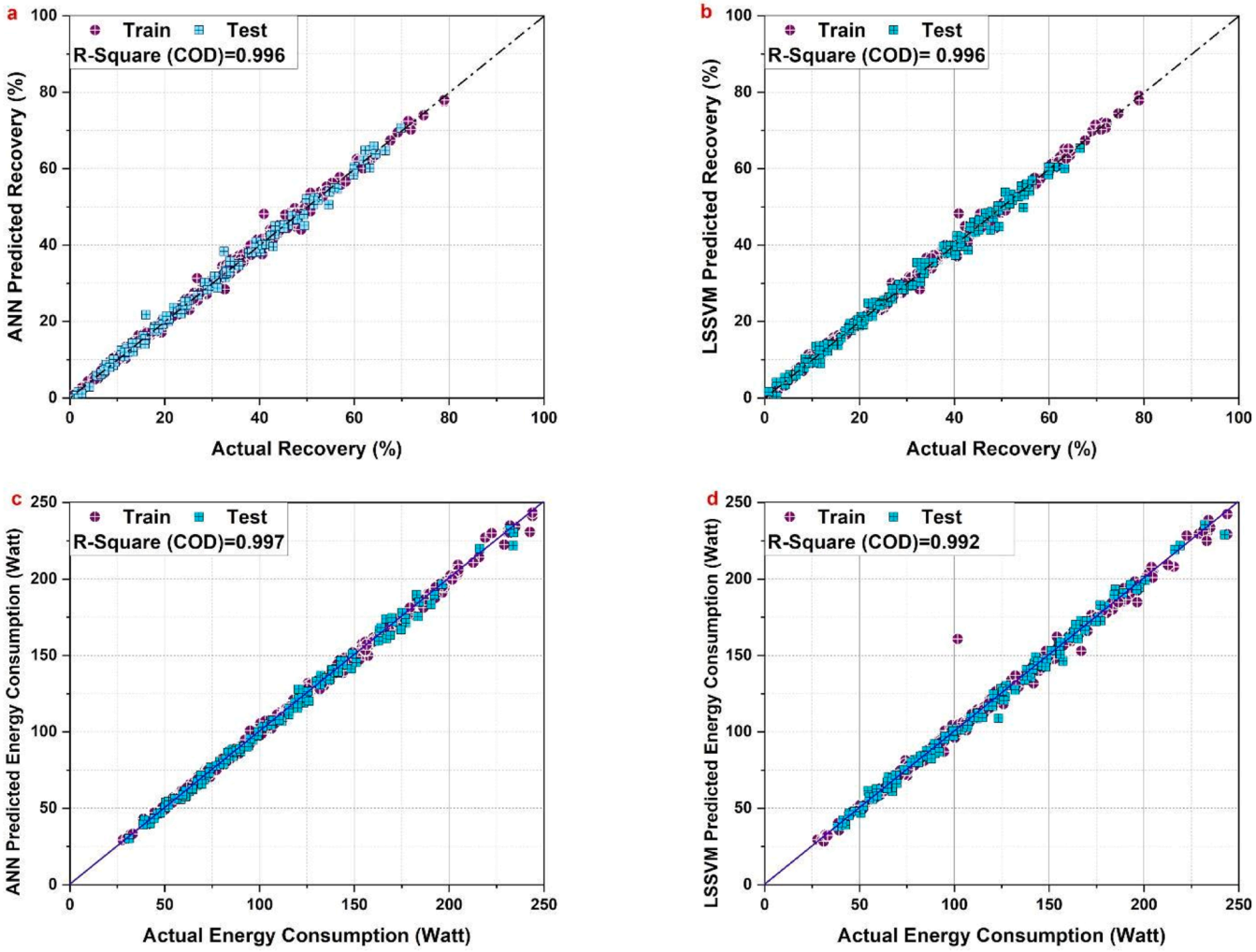

Fig. 5. Experimental data (i.e., actual data) of EC and *Re* are compared to the values obtained from the developed models for (a) ANN-*Re*, (b) LSSVM-*Re*, (c) ANN-EC, and (d) LSSVM-EC. The comparison reveals that all the predictions have R^2 values higher than 0.99, signifying accurate predictions using both methods.

predicted specific energy consumption (SEC, EC per unit permeate flow rate), *Re*, and EC, achieving $R^2 > 0.9$ (Section 4.3, (Abkar, 2015)) considering interaction terms (e.g., pressure × flow rate, pressure × flow rate × temperature, $p < 0.05$), offering a comprehensive analysis beyond correlation. The ANN, with a multi-output architecture (5 inputs, three hidden layers with 32–64–32 neurons, ReLU activation, 0.1 dropout), outperforms linear regression ($R^2 > 0.9$, Abkar, 2015) and RSM (15–25 % errors) by capturing nonlinear EC-*Re* dynamics.

Fig. 6 presents model errors: (a) RMSE and (b) AARE % for training and testing datasets. For *Re*, LSSVM outperformed ANN, with total RMSE

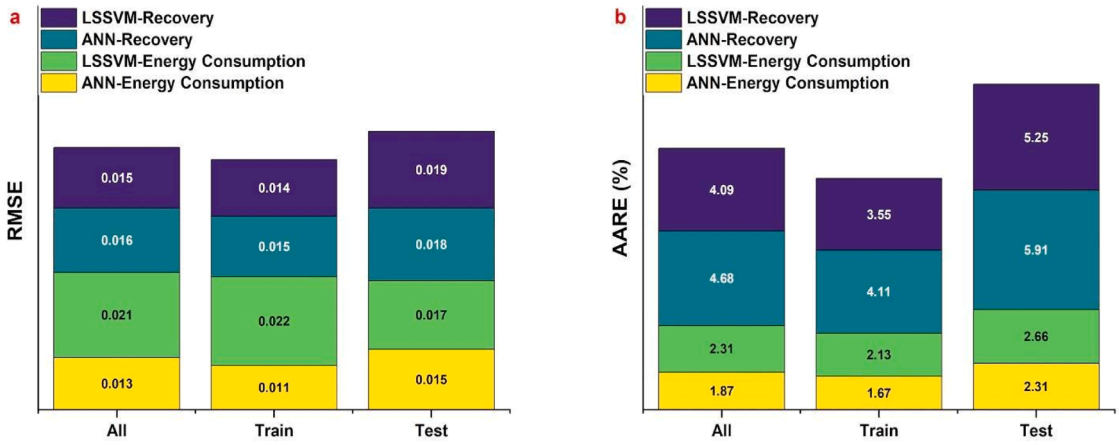

Fig. 6. The models' errors are demonstrated based on (a) root mean square error (RMSE) and (b) average absolute relative error (AARE) of the ANN and LSSVM models for *Re* and EC. This analysis indicates that the ANN model provides better predictions for EC, whereas the LSSVM model performs more effectively for *Re*.

= 0.015 (training: 0.014, testing: 0.016) vs. ANN's 0.016 (training: 0.015, testing: 0.017), and AARE % = 4.09 % (training: 4.11 %, testing: 5.24 %) vs. ANN's 4.69 % (training: 4.11 %, testing: 5.91 %). For EC, ANN showed better performance, with total RMSE = 0.013 (training: 0.011, testing: 0.015) vs. LSSVM's 0.021 (training: 0.022, testing: 0.020), and AARE % = 1.88 % (training: 1.67 %, testing: 2.31 %) vs. LSSVM's 2.30 % (training: 2.13 %, testing: 2.66 %). These results further highlight ANN's strength in capturing EC's nonlinear dynamics and LSSVM's robustness for *Re*, particularly in BWRO systems where high *Re* rates (75–85 %) is desired hence scaling effects are pronounced (Wilf and Bartels, 2005).

Model validation was conducted using an independent dataset not used in training, ensuring robustness across diverse operating conditions. Fig. 7 presents validation results: (a) ANN-predicted vs. actual EC, and (b) LSSVM-predicted vs. actual *Re*. The close match between predicted and experimental values demonstrates that the ANN and LSSVM algorithms effectively capture the dynamic and nonlinear relationships of EC and *Re* across varying input conditions, enabling engineers to accurately predict BWRO performance in real-world scenarios with complex operational challenges. These validation results are quantitatively detailed in Table 3a, which highlights ANN's superior EC prediction (R^2 = 0.997, RE % = 0.10 %, AARE % = 1.88 %, RMSE = 0.013) and LSSVM's robust *Re* prediction (R^2 = 0.996, RE % = −0.01 %, AARE % = 4.09 %, RMSE = 0.015) compared to RSM (e.g., AK-EC: R^2 = 0.897, AARE % = 21.21 %).

To ensure model reliability, overfitting was assessed by monitoring the ANN learning curve (Fig. S4), which shows a steady decrease in test error without divergence from training error, indicating effective generalization. This absence of overfitting confirms that the AI models can reliably predict EC and *Re* across varied BWRO conditions, enhancing confidence in their applicability to real-world desalination systems.

These results underscore the efficacy of AI-based models in handling BWRO's complex dynamics, such as variable interactions and scaling risks, compared to RSM's limitations (Table 3b). ANN's ability to model EC aligns with its sensitivity to feed flow rate and pressure (Section 3.1, RF = 31.3 %, 28.6 %), while LSSVM's strength in *Re* prediction supports its use for optimizing membrane performance (Stover, 2004). These findings inform the multi-objective optimization.

3.4. Multi objective optimization using NSGA-II approach

Multi-objective optimization was conducted using the Non-dominated Sorting Genetic Algorithm II (NSGA-II) to systematically identify Pareto-optimal operating conditions for the BWRO system by simultaneously minimizing specific EC and maximizing water *Re*. Building on the ANN models validated in Section 3.3 for their high predictive accuracy (R^2 = 0.997 for EC and R^2 = 0.996 for *Re*), these surrogates were integrated directly as objective functions within the NSGA-II framework. The algorithm was configured with a population size of 100 and 200 generations, employing simulated binary crossover and polynomial mutation operators to evolve feasible solutions. Both objectives were framed for minimization by defining the second objective as 1–*Re*, with an operational constraint capping *Re* at 80 % to mitigate scaling risks such as calcium carbonate precipitation (Tong and Elimelech, 2016).

Table 3b
Summarized statistical analyses for the ANN, LSSVM, and quadratic models.

		R^2	RE (%)	AARE (%)	RMSE
ANN	*Re*	0.996	−0.9690	4.69	0.016
	EC	0.997	0.0978	1.88	0.013
LSSVM	*Re*	0.996	−0.007	4.09	0.015
	EC	0.992	−0.162	2.30	0.021
RSM	AG - *Re*	0.968	−10.60	15.92	0.058
	AG - EC	0.986	23.34	23.35	0.076
	AK - *Re*	0.930	14.86	22.70	0.131
	AK - EC	0.897	−21.21	27.60	0.137

For the ANN models, we began with a simple architecture consisting of a single hidden layer (5–32–2), inspired by previous studies (Prakash Maran et al., 2013). The number of hidden layers was gradually increased until the validation accuracy no longer improved, resulting in a three-hidden-layer architecture (5–32–64–32–2) being selected as optimal. We explored learning rates in the range of {1×10^{-3}, 3×10^{-3}, 1×10^{-2}}, weight decay values of {1×10^{-5}, 1×10^{-4}, 1×10^{-3}}, and batch sizes of (Keshtegar et al., 2019; Nour-Mohammad and Fakhroleslam, 2025; Breiman, 1996).

For the NSGA-II algorithm, key parameters such as population size and number of generations were determined in a similar empirical manner. The optimization started with a population size of 100, which was subsequently increased to 150 and 400 to assess convergence behavior. When the Pareto front stabilized, a population size of 100 and 200 generations were deemed sufficient. We employed a simulated binary crossover operator with a probability of 0.9 and a tournament selection mechanism in each generation to preserve solution diversity.In contrast to earlier works that often employed conventional multi-

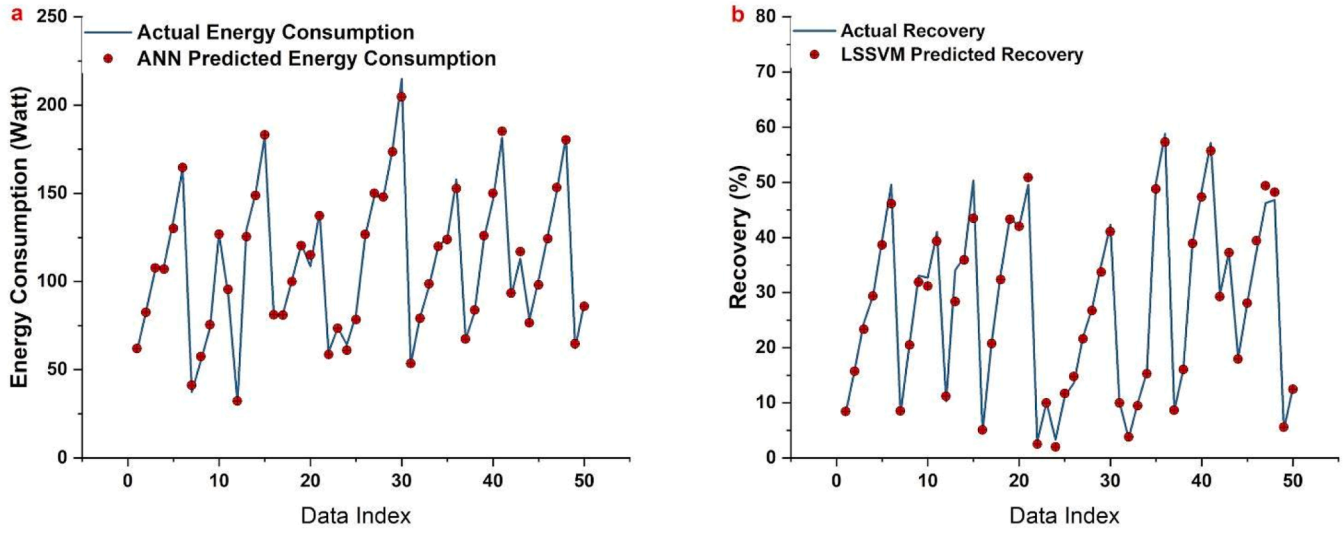

Fig. 7. The model's performance is validated by showcasing (a) actual EC and ANN-predicted EC, as well as (b) actual *Re* versus LSSVM-predicted *Re*. Models with an R2 value exceeding 0.99 exhibit strong predictive capabilities.

objective optimization frameworks for BWRO design, such as Vince et al. (2008), Lu et al. (2007) or on single-objective and Djebedjian et al. (2008) optimization, this study advances operational-level multi--objective optimization by embedding empirically trained ANN surrogates within the NSGA-II scheme specifically for brackish water conditions. Vince et al. (2008) demonstrated a mixed-integer nonlinear programming (MINLP) approach for optimizing BWRO configurations, balancing cost, energy use, and environmental indicators, but did not integrate data-driven models for real-time prediction of energy–recovery trade-offs under operational fouling constraints (Vince et al., 2008). Similarly, Lu et al. (2007) applied a process synthesis approach to RO system design under different feed concentrations but focused primarily on structural configuration and cost minimization rather than direct ANN-based energy–recovery performance mapping (Lu et al., 2007). Compared to Guria et al. (2005) (Guria et al., 2005), who first applied NSGA-II to brackish water RO systems to generate Pareto-optimal sets for module design and basic operational settings, this study extends the framework by shifting the focus from static design variables to dynamic operational conditions optimized through empirically trained ANN surrogates. Guria et al. demonstrated that for existing BWRO plants, the operating pressure difference (ΔP) was essentially the sole adjustable parameter, with membrane area and type treated as fixed constraints. In contrast, the present work leverages a multi-input ANN model that captures the coupled effects of feed flow rate, pressure, temperature, salinity, and membrane type on specific EC and *Re*, allowing the NSGA-II to explore a broader and more realistic solution space (Guria et al., 2005). This approach explicitly integrates practical fouling and scaling limits into the feasible region, producing numerically verified Pareto fronts (Fig. 8) that identify low-energy, high--recovery combinations not accessible through parameterized models alone. While Guria et al. validated their algorithmic variants (NSGA-II-JG, NSGA-II-aJG) for convergence speed and general solution diversity, they did not link their multi-objective trade-offs to pilot-scale empirical data or advanced AI surrogates. This study bridges that gap by coupling a proven evolutionary algorithm with high-fidelity surrogate models to deliver actionable setpoints for real-time BWRO plant operation under variable feed conditions.

As illustrated in Fig. 8, the feasible solution space predicted by the ANN model (green region) closely bounds the Pareto-optimal front (blue dots), demonstrating that the optimal trade-offs cluster in a narrower band of moderate feed flow rates and pressures. Unlike classical RSM or parametric flux models that assume constant scaling factors or ideal membrane conditions, this study's data-driven Pareto front, grounded real data, captures practical nonlinearities and trade-offs that prior parametric or polynomial flux models cannot resolve. Fig. 9 further reveals how the key operational parameters shape these trade-offs: feed flow rate and pressure dominate EC outcomes (RF = 31.3 % and 28.6 %), while membrane type and flow rate jointly exert the highest influence on *Re* (RF = 32.2 % and 30.2 %). This quantification aligns with the sensitivity trends highlighted earlier and extends insights beyond previous studies such as Djebedjian et al. (2008); Sadri et al. (2016); Dologlu and Sildir (2022), providing numerically explicit operating regions that maintain high recoveries without breaching scaling thresholds. The five panels show how feed flow rate, operating pressure, salinity, temperature, and membrane type distribute across the Pareto-optimal front. The color gradients reveal that regions achieving lower EC and higher *Re* (for single pass-single stage BWRO) correspond to low-to-moderate feed flow rates between 3–4.5 LPM, pressures in the range of 90–125 psi, and slightly elevated feed temperatures. The temperature surface shows that the optimal region for maximizing *Re* while maintaining low EC corresponds to feed temperatures between 33–37 °C. Within this range, the solution space clusters around higher *Re* (>50 %) at moderate energy levels (~80–120 W), confirming that slight pre-heating of feedwater can improve membrane flux without breaching scaling constraints. Higher salinity zones shift the feasible region toward higher EC and lower *Re*, as expected due to increased osmotic pressure. The salinity surface (Fig. 9c) indicates that for the studied BWRO configuration, the optimum operational region for simultaneously minimizing specific EC and maximizing *Re* clusters around feed salinity levels of 2500–3200 ppm. At higher salinity levels (above ~3500 ppm), the feasible solution space shifts predictably toward increased energy demand and slightly lower *Re* due to higher osmotic pressures. However, the Pareto front remains valid for these conditions, demonstrating that the ANN–NSGA-II framework can identify adjusted trade-offs and practical setpoints for more saline brackish sources when required, albeit with higher operating pressure and careful scaling management. The membrane type map confirms that the AK2540TM membrane, which has higher permeability than AG2540TM, dominates the optimal low-EC, high-*Re* region (orange) by enabling an additional 5–8 % *Re* gain at comparable energy levels. This comparison demonstrates that the combined tuning of flow rate, pressure, and membrane selection within these ranges defines the practical operating regions for maximizing BWRO performance while respecting single-stage, single-pass design limits and controlling for scaling risk. The consolidated parameter maps thus translate the ANN–NSGA-II multi-objective results into a quantifiable optimum envelope for robust brackish water desalination, as illustrated in Fig. 9, which visualizes these optimum regions for practical process monitoring and control.

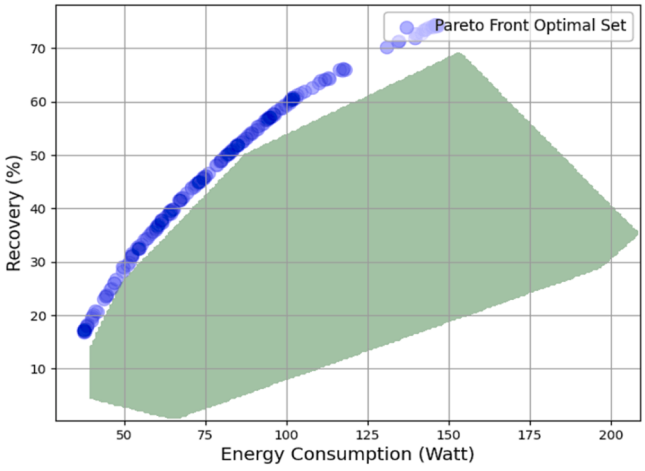

Fig. 8. Pareto front obtained by NSGA-II for minimizing EC and maximizing *Re*, overlaid on the feasible solution space predicted by the ANN model. The green area represents feasible operating conditions, while the blue dots (●) on the upper side of the feasible region denote Pareto-optimal solutions defining the best trade-offs between energy use (EC) and *Re* for the BWRO system.

A key outcome of the ANN–NSGA-II framework is that it reveals practical operating conditions under which *Re* can be safely increased from the nominal factory baseline of 15 % to 50–80 % without exceeding or even while slightly reducing the standard test pressures of 225 psi for AG and 115 psi for AK membranes. This is made possible by simultaneously tuning multiple interacting variables: increasing feed flow rate enhances shear at the membrane surface, which reduces concentration polarization and allows higher flux at a given pressure; moderate feed heating (to 33–37 °C) lowers water viscosity and raises membrane permeability, further boosting flux; and selecting membranes with inherently higher water permeability (e.g., AK2540TM) shifts the feasible region toward higher *Re* at equal or lower net driving pressure. By capturing these coupled, nonlinear effects, the ANN–NSGA-II approach shows that *Re* can be raised by a factor of three to five while unit specific EC drops significantly compared to the factory test point. This demonstrates that real brackish water RO systems can operate far beyond nominal design conditions when operational parameters are intelligently co-optimized, a result that classical polynomial or parametric flux models cannot resolve due to oversimplified assumptions and fixed single-variable trade-offs.

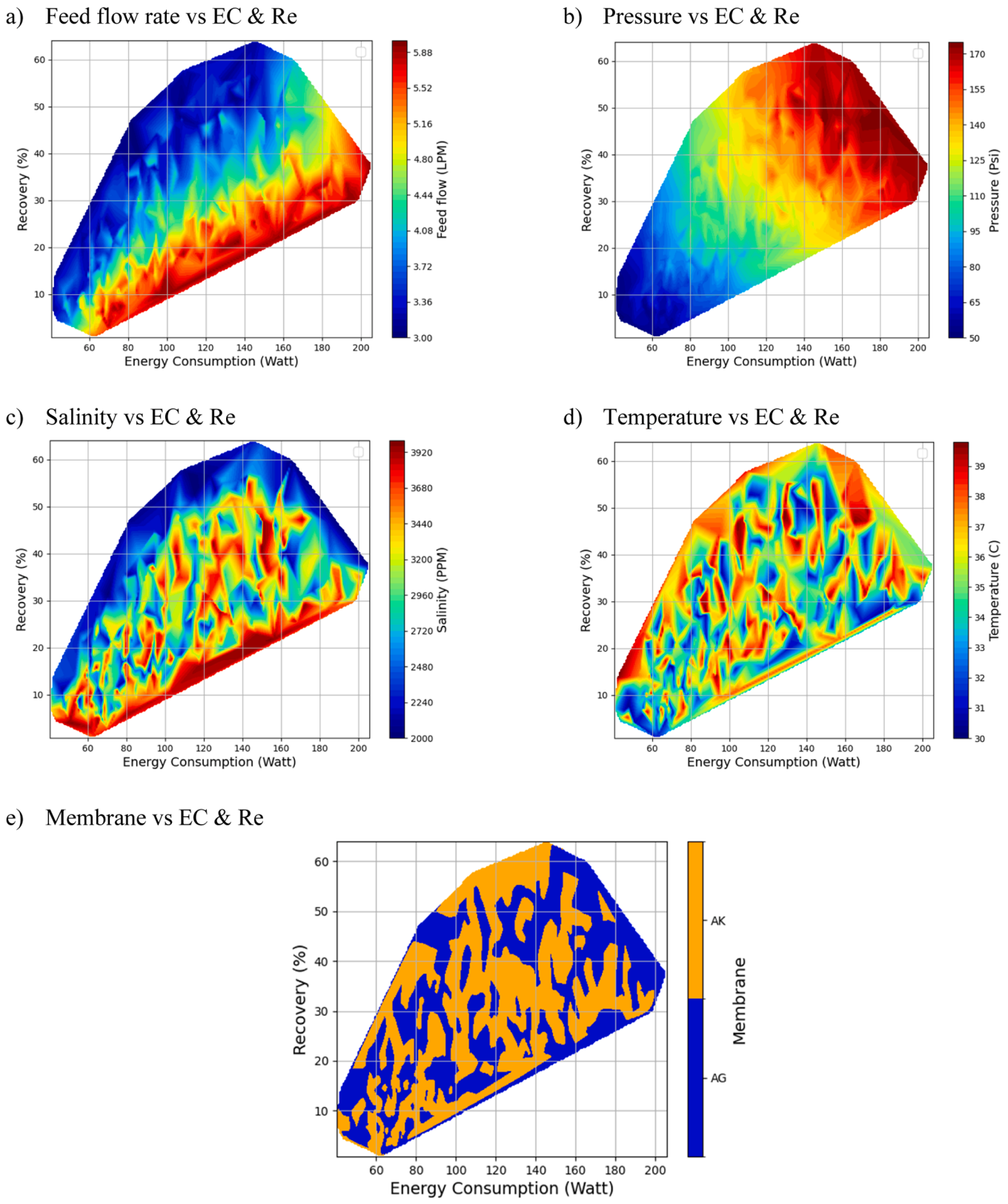

Fig. 9. Three-dimensional response surfaces showing the distribution of key input parameters within the feasible solution space for energy consumption (EC, W) and recovery (*Re*, %), derived from NSGA-II optimization using ANN surrogates. Subfigures are: (a) Feed flow rate (LPM) vs. EC & *Re*, (b) Pressure (psi) vs. EC & *Re*, (c) Salinity (ppm) vs. EC & *Re*, (d) Temperature (°C) vs. EC & *Re*, (e) Membrane type (AG and AK) vs. EC & *Re*. The color legend in each subfigure indicates the parameter value range (e.g., feed flow rate 3–6 LPM, temperature 33–37 °C) and performance levels (EC and *Re*), with upper side of feasible region representing the of Pareto-optimal solutions, enabling identification of optimal operating zones (e.g., temperature 33–37 °C for $Re > 50$ %).

To quantify the practical benefit of the optimized operating regions, the specific energy consumption (SEC) of the system was calculated using standard RO design equations (see SI- S2.3). The factory testing conditions for the AG and AK membranes specify nominal feed pressures of 225 psi (1551 kPa) and 115 psi (793 kPa) at a fixed *Re* of only 15 %, reflecting typical manufacturer baseline points for flux and rejection characterization. In contrast, the ANN–NSGA-II framework identifies feasible operating conditions that increase *Re* to 50–80 % while reducing or moderating net driving pressure to 90–125 psi. Because specific energy in RO is inversely proportional to *Re* fraction, this increase in *Re* substantially lowers SEC requirements even when absolute pressure remains similar or slightly lower. For example, for the AG membrane, increasing *Re* from 15 % to 50 % at moderate pressure can reduce SEC from ~1.03 kWh/m³ to ~0.38 kWh/m³ when excluding potential long-term fouling or membrane aging losses, corresponding to a unit energy reduction of >50 %. This confirms that combining high-fidelity surrogate modeling with multi-objective optimization can reliably translate nominal design data into realistic, operationally achievable energy reductions, which older static optimization approaches cannot fully capture due to fixed-point assumptions and limited input dynamics.

Fig. 10 deepens this perspective by comparing the modeled solution spaces for both membranes (AG and AK) against experimental data and manufacturer specifications. The close fit of the ANN predictions (AARE % = 1.88–4.69 %) relative to RSM (AARE % = 10.60–23.34 %) reinforces the ANN's capability to resolve the complex nonlinear interactions between salinity, flow, and membrane properties. This is particularly significant for AK2540TM, where the RSM's tendency to over- or underpredict EC is more pronounced due to unmodeled permeate flux behaviors under variable fouling conditions.

Despite these strengths, certain limitations must be acknowledged. As with any evolutionary algorithm, NSGA-II's stochastic search is sensitive to initial population seeding and may converge prematurely to local optima if solution diversity is not preserved through crowding distance management (Deb et al., 2002). Computational demand is also non-negligible: the integration of surrogate models like ANN means each generation requires multiple forward passes through a nonlinear model, which scales computational cost with increasing population size and generation count (Nour-Mohammad and Fakhroleslam, 2025).

Furthermore, while the present ANN models robustly capture BWRO dynamics for the tested membrane chemistries, extending this approach to next-generation materials such as graphene oxide or advanced thin-film composites (Skuse et al., 2021; Boretti and Rosa, 2019) would require new training datasets to preserve predictive fidelity under different fouling, scaling, and permeability regimes.

Practically, the actionable setpoints derived here—such as operating within 3–4.5 LPM feed flow and 90–125 psi pressure ranges using AK2540TM—provide clear guidelines for operators to tune pump loads, membrane staging, and antiscalant dosing to maintain high *Re* at minimized EC. Since membrane processes account for >50 % of total desalination operating expenses (N. Voutchkov, 2018), even modest EC reductions of 10–15 % can translate into significant operational cost savings and proportional cuts in greenhouse gas emissions, estimated at 0.1–0.2 kg CO_2 eq/m³ (Stokes and Horvath, 2009). A grid emission factor of 0.85–1.0 kg CO_2/kWh was assumed, consistent with typical BWRO energy LCA studies (Stokes and Horvath, 2009; N. Voutchkov, 2018). Additionally, the modularity of this framework enables its adaptation to seawater RO or hybrid nanofiltration–RO configurations by retraining the underlying ANN models with higher-salinity datasets and reconfiguring constraints to address osmotic pressure and biofouling risks, extending its relevance for diverse brackish or saline water sources under increasing water scarcity and climate pressures.

3.5. Compare to the single objective optimization problem modeling

To further assess optimization performance, we reframed the problem as a single-objective task using an ensemble-based multi-input single-output (MISO) ANN and compared it with the multi-objective scheme. In the single-objective formulation, we first trained two independent ANN regressors—one to predict *Re* and the other to predict energy consumption (EC)—using the same dataset. Their outputs were then combined into a scalar objective:

$$J(x) = \frac{EC(x)}{Re(x)} \quad \text{(i)}$$

Where x denotes the input parameters to be optimized. Next, we adopted a MISO ensemble by constructing a bagging model with bootstrap sampling (Breiman, 1996). The ensemble comprised 7 weak learners, each an MLP regressor with a hidden-layer configuration of (8, 16, 8). The base learners were intentionally kept only moderately accurate (i.e., "weak") to leverage variance reduction under bagging (Breiman, 1996). We then wrapped the fitted ensemble as a black-box objective for a GA with population size = 150, selecting GA

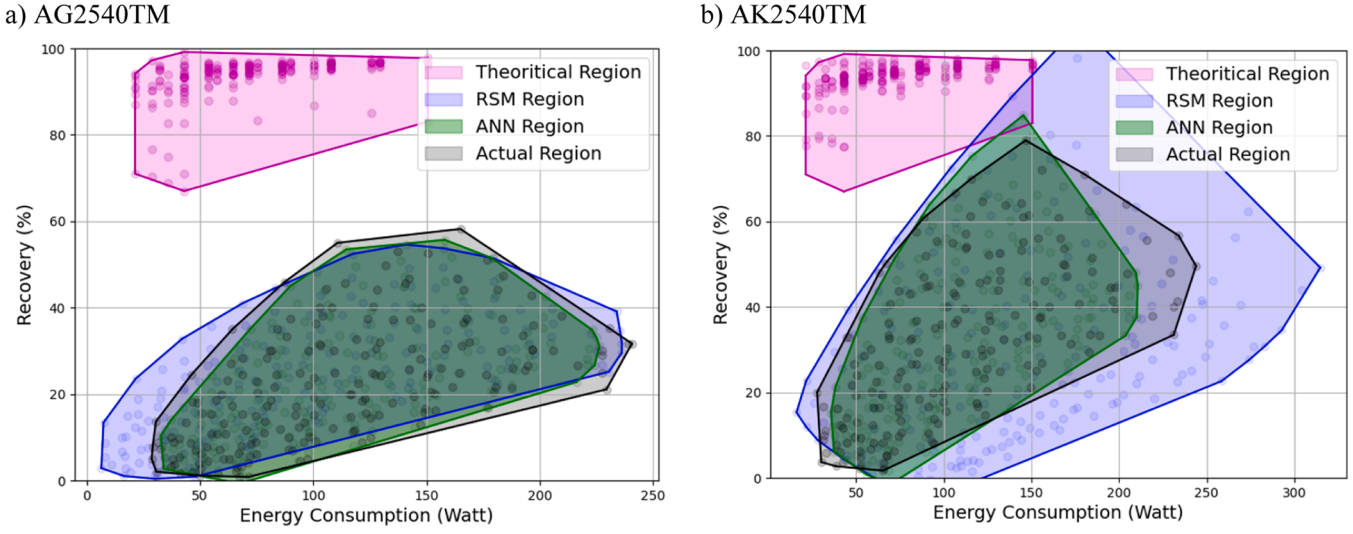

Fig. 10. Comparison of modeled solution spaces for AG2540TM (a) and AK2540TM (b) membranes. Theoretical performance regions (pink) are based on manufacturer specifications; RSM Regions (blue) and ANN Regions (green) show solution spaces predicted by Response Surface Method and Artificial Neural Network models, respectively. The Actual Region (gray) represents the envelope of experimental data. The ANN models closely match the experimental data for both membranes, especially for the higher-permeability AK membrane, capturing feasible high-*Re*, low-energy conditions that the RSM model overestimates or underfits.

parameters empirically from a predefined grid to achieve the best observed performance. Code and data for this experiment are available in our GitHub repository (multi_input_single_output_ANNs.py). The GA run produced the following best configuration (minimizing $J(x)$), which simultaneously reduces EC while increasing *Re* (Table 4).

In contrast, the NSGA-II multi-objective approach yielded a Pareto set of 100 solutions, each expressing a distinct trade-off between recovery and energy use. This front provides flexibility to select configurations aligned with practical priorities and system constraints (sample solutions in Table 5).

4. Conclusion

This study addresses the urgent need for resilient and cost-effective brackish water desalination by advancing both performance prediction and operational optimization through an integrated AI-driven approach. The AI–NSGA-II framework addresses a critical gap in prior RO studies, which often rely on single-objective optimization ((Djebedjian et al., 2008), single-output ANN prediction models ((Mahadeva et al., 2023), or static NLP methods (Vince et al., 2008; Lu et al., 2007). By integrating a multi-output ANN, trained on pilot-scale BWRO data, with NSGA-II, our approach captures nonlinear interactions between energy consumption and recovery, generating a Pareto-optimal operating region that adapts to dynamic conditions like salinity variations and membrane fouling. This multi-objective framework provides flexible operational setpoints, enhancing BWRO sustainability and resilience compared to conventional approaches.

Sensitivity analyses revealed that membrane *Re* is primarily governed by membrane selection (32.2 %) and feed flow rate (30.2 %), while specific energy consumption is driven mainly by feed flow rate (31.3 %) and pressure (28.6 %). In contrast to traditional polynomial fitting or response surface methodologies—whose absolute average relative errors can exceed 15–25 % and which often assume constant or idealized conditions—this ANN-based framework achieves predictive accuracies exceeding $R^2 = 0.99$ across validation datasets.

Compared to regression models from our prior work Abkar(2015), Abkar et al. (2024), which predicted specific energy consumption (SEC, EC per unit permeate flow rate) and *Re* ($R^2 > 0.9$), the ANN achieves superior accuracy ($R^2 > 0.99$, AARE < 5 %,). However, the ANN's simple architecture may limit generalization to complex, multi-device setups, a focus for future work involving deeper models or transfer learning.

The optimization framework presented, validated on a single-stage BWRO pilot plant with AG2540TM and AK2540TM membranes, demonstrates significant potential for broader application. The ANN—NSGA-II approach is modular and can be extended to industrial-scale multi-stage RO systems by retraining the ANN with datasets incorporating inter-stage pressures, permeate staging ratios, and energy recovery device (ERD) efficiencies. This adaptation would adjust the objective functions to address stage-specific constraints, such as scaling across membranes, while leveraging the NSGA-II's scalable search (Section 2.4.2). The sensitivity analysis (Section 3.1) suggests focusing on pressure and flow rate optimization in multi-stage designs, offering a foundation for future industrial validation and sustainable water management.

The integrated ANN–NSGA-II method not only generates reliable Pareto-optimal fronts but also provides a practical *operating region* rather than a single restrictive optimum point. This optimum region can be directly translated into dynamic control strategies that accommodate real-world variations in feedwater salinity, seasonal temperature shifts, equipment wear, and membrane fouling. Such flexibility ensures that BWRO systems can consistently operate at low specific energy consumption and high *Re*, yielding tangible operational savings and significant CO_2 footprint reductions.

By overcoming the static limitations of earlier design-stage optimizations—such as those constrained to fixed pressures or static module geometries—this study demonstrates how AI-enhanced multi-objective optimization can deliver actionable, adaptable setpoints for real-time plant operation. This adaptability is critical for practical engineering control systems, which cannot reliably lock a plant to a single theoretical optimum but can track within a robust optimum *region*. In addition, the framework's ANN and LSSVM models were benchmarked against RSM to verify prediction accuracy, ensuring the optimized region is grounded in robust empirical validation. All models and underlying code are openly available to maximize reproducibility and practical uptake.

Overall, the framework established here underscores how AI-enabled, data-driven optimization can push brackish water desalination closer to true sustainability. By providing operators with validated, flexible operating envelopes, this approach supports the delivery of affordable, low-carbon, high-recovery desalinated water, helping communities address escalating water scarcity and climate resilience challenges with practical, field-ready tools. By systematically validating that practical recoveries can be boosted from nominal factory test points of around 15 % to 50–80 % while maintaining moderate operating pressures, this study quantifies the real unit energy savings (>50 %) achievable through integrated AI-guided operation. While the short-term performance confirms this benefit, future studies should extend the framework to long-term monitoring to fully capture membrane aging and irreversible fouling effects in real plants. All models and code are made openly available to ensure reproducibility and accelerate practical adoption.

Table 4
Best solution obtained by GA optimization of ensemble of MLP regressors.

Feed flowrate (LPM)	Temperature (°C)	Salinity (ppm)	Pressure (psi)	Membrane	EC (watt)	*Re*
3.0	40.0	2000	107.25	AG	74.4	0.45

Table 5
Pareto optimal sample solutions found by NSGAII in multi objective optimization approach.

Feed flowrate (LPM)	Temperature (°C)	Salinity (ppm)	Pressure (psi)	Membrane	EC (watt)	*Re*
6.0	40	3000	75	AG	88.5	0.34
6.0	40	2000	150	AG	178.0	0.61
6.0	40	3000	100	AG	97.3	0.37
…	…	…	…	…	…	…

Funding

The funding for this study was provided by the American Water Works Association and Natural Sciences and Engineering Research Council of Canada-Postdoctoral Fellowship awarded to Dr. Leili Abkar in two separate phases.

CRediT authorship contribution statement

Leili Abkar: Writing – review & editing, Writing – original draft, Visualization, Project administration, Methodology, Data curation, Conceptualization. **Shima Kamyab:** Writing – review & editing, Writing – original draft, Visualization, Software, Data curation. **Amirreza Aghili Mehrizi:** Writing – review & editing, Writing – original draft, Visualization, Software, Data curation. **Pezhman Abbasi:** Writing – review & editing, Writing – original draft, Visualization, Software. **Mark van Loosdrecht:** Writing – review & editing, Writing – original draft, Supervision. **Abbas Ghassemi:** Writing – review & editing, Supervision, Funding acquisition. **Madjid Mohseni:** Writing – review & editing, Supervision.

Declaration of competing interest

The authors declare that they have no known competing financial interests or personal relationships that could have appeared to influence the work reported in this paper.

Acknowledgment

The authors would like to acknowledge the help and contributions of Karl Dykeman for designing and building the BWRO setup and Mr. John Piechel from GE for generously providing the membranes. We also would like to thank Professor Trevor Campbell- UBC for his time reviewing the machine learning techniques and modeling.

Supplementary materials

Supplementary material associated with this article can be found, in the online version, at doi:10.1016/j.watres.2025.124934.

Data availability

Data will be made available on request.

References

Abkar, L., Aghili Mehrizi, A., Jafari, M., Beck, S.E., Ghassemi, A., Van Loosdrecht, M.C. M., 2024. Optimizing energy efficiency in brackish water reverse osmosis (BWRO): a comprehensive study on prioritizing critical operating parameters for specific energy consumption minimization. Sci. Total Environ. 932, 172772. https://doi.org/10.1016/J.SCITOTENV.2024.172772.

Abkar: Energy consumption optimization of a brackish... - google scholar, https://scholar.google.com/scholar?cluster=14050494331917507080&hl=en&oi=scholarr.

Adda, A., Hanini, S., Bezari, S., Laidi, M., Abbas, M., 2022. Modeling and optimization of small-scale NF/RO seawater desalination using the artificial neural network (ANN). Environ. Eng. Res. 27. https://doi.org/10.4491/eer.2020.383.

Al-Obaidi, M.A., Filippini, G., Manenti, F., Mujtaba, I.M., 2019. Cost evaluation and optimisation of hybrid multi effect distillation and reverse osmosis system for seawater desalination. Desalination 456, 136–149. https://doi.org/10.1016/J.DESAL.2019.01.019.

Alardhi, S.M., Salman, A.D., Breig, S.J.M., Jaber, A.A., Fiyadh, S.S., AlJaberi, F.Y., Duc Nguyen, D., Van, B., Le, P.C., 2024. Artificial neural network and response surface methodology for modeling reverse osmosis process in wastewater treatment. J. Ind. Eng. Chem. 133, 599–613. https://doi.org/10.1016/J.JIEC.2024.02.039.

Amer, A.Y.A., 2023. Global-local least-squares support vector machine (GLocal-LS-SVM). PLoS One 18, e0285131. https://doi.org/10.1371/JOURNAL.PONE.0285131.

Antipova, E., Boer, D., Cabeza, L.F., Guillén-Gosálbez, G., Jiménez, L., 2013. Multi-objective design of reverse osmosis plants integrated with solar Rankine cycles and thermal energy storage. Appl. Energy. 102. https://doi.org/10.1016/j.apenergy.2012.06.038.

Behzadi, A., Gholamian, E., Alirahmi, S.M., Nourozi, B., Sadrizadeh, S., 2022. A comparative evaluation of alternative optimization strategies for a novel heliostat-driven hydrogen production/injection system coupled with a vanadium chlorine cycle. Energy Convers. Manag. 267. https://doi.org/10.1016/j.enconman.2022.115878.

Boretti, A., Rosa, L., 2019. Reassessing the projections of the world water development report. NPJ Clean Water 2. https://doi.org/10.1038/s41545-019-0039-9.

Boretti, A., Al-Zubaidy, S., Vaclavikova, M., Al-Abri, M., Castelletto, S., Mikhalovsky, S.: Outlook for graphene-based desalination membranes, (2018).

Breiman, L., 1996. Bagging predictors. Mach. Learn. 24, 123–140. https://doi.org/10.1007/BF00058655/METRICS.

Brooke, R., Fan, L., Khayet, M., Wang, X., 2022. A complementary approach of response surface methodology and an artificial neural network for the optimization and prediction of low salinity reverse osmosis performance. Heliyon 8. https://doi.org/10.1016/j.heliyon.2022.e10692.

Cai, M., Hocine, O., Mohammed, A.S., Chen, X., Amar, M.N., Hasanipanah, M., 2022. Integrating the LSSVM and RBFNN models with three optimization algorithms to predict the soil liquefaction potential. Eng. Comput. 38. https://doi.org/10.1007/s00366-021-01392-w.

Chan, M.K., Shams, A., Wang, C.C., Lee, P.Y., Jahani, Y., Mirbagheri, S.A., 2023. Artificial neural network model for membrane desalination: a predictive and optimization study. Computation 11. https://doi.org/10.3390/computation11030068.

Deb, K., Pratap, A., Agarwal, S., Meyarivan, T., 2002. A fast and elitist multiobjective genetic algorithm: NSGA-II. IEEE Trans. Evol. Comput. 6, 182–197. https://doi.org/10.1109/4235.996017.

DeNicola, E., Aburizaiza, O.S., Siddique, A., Khwaja, H., Carpenter, D.O., 2015. Climate change and water scarcity: the case of Saudi Arabia. Ann. Glob. Heal. 81, 342–353. https://doi.org/10.1016/J.AOGH.2015.08.005.

Djebedjian, B., Gad, H., Khaled, I., Rayan, M.A.: Optimization of Reverse Osmosis desalination system using genetic algorithms technique. 12, (2008).

Dologlu, P., Sildir, H., 2022. Data driven identification of industrial reverse osmosis membrane process. Comput. Chem. Eng. 161, 107782. https://doi.org/10.1016/J.COMPCHEMENG.2022.107782.

Du, Y., Xie, L., Liu, Y., Zhang, S., Xu, Y., 2015. Optimization of reverse osmosis networks with split partial second pass design. Desalination 365. https://doi.org/10.1016/j.desal.2015.03.019.

Foroughi, M., Rahmani, A.R., Asgari, G., Nematollahi, D., Yetilmezsoy, K., Samarghandi, M.R., 2020. Optimization and modeling of tetracycline removal from wastewater by three-dimensional electrochemical system: application of response surface methodology and least squares support vector machine. Environ. Model. Assess. 25. https://doi.org/10.1007/s10666-019-09675-9.

Ghaedi, M., Ghaedi, A.M., Hossainpour, M., Ansari, A., Habibi, M.H., Asghari, A.R., 2014. Least square-support vector (LS-SVM) method for modeling of methylene blue dye adsorption using copper oxide loaded on activated carbon: kinetic and isotherm study. J. Ind. Eng. Chem. 20. https://doi.org/10.1016/j.jiec.2013.08.011.

Ghanbari, K., Maleki, A., Rezaei Ochbelagh, D., 2024. Optimal design of solar/wind/energy storage system-powered RO desalination unit: single and multi-objective optimization. Energy Convers. Manag. 315, 118768. https://doi.org/10.1016/J.ENCONMAN.2024.118768.

Guria, C., Bhattacharya, P.K., Gupta, S.K., 2005. Multi-objective optimization of reverse osmosis desalination units using different adaptations of the non-dominated sorting genetic algorithm (NSGA). Comput. Chem. Eng. 29. https://doi.org/10.1016/j.compchemeng.2005.05.002.

Habieeb, A.R., Kabeel, A.E., Sultan, G.I., Abdelsalam, M.M., 2023. Advancements in water desalination through artificial intelligence: a comprehensive review of AI-based methods for reverse osmosis membrane processes. Water Conserv. Sci. Eng. 8, 1–18. https://doi.org/10.1007/S41101-023-00227-7/FIGURES/6.

Hamza, K., Shalaby, M., Nassef, A.O., Aly, M.F., Saitou, K., 2011. Studies on the design of reverse osmosis water desalination systems for cost and energy efficiency. Proc. ASME Des. Eng. Tech. Conf. 1, 665–675. https://doi.org/10.1115/DETC2010-28493.

Hemmati-Sarapardeh, A., Varamesh, A., Husein, M.M., Karan, K.: On the evaluation of the viscosity of nanofluid systems: modeling and data assessment, (2018).

Jawad, J., Hawari, A.H., Javaid Zaidi, S.: Artificial neural network modeling of wastewater treatment and desalination using membrane processes: a review, (2021).

Jones, E., Qadir, M., van Vliet, M.T.H., Smakhtin, V., Kang, S.mu: The state of desalination and brine production: a global outlook, (2019).

Kardani, M.N., Baghban, A., Sasanipour, J., Mohammadi, A.H., Habibzadeh, S., 2018. Group contribution methods for estimating CO2 absorption capacities of imidazolium and ammonium-based polyionic liquids. J. Clean. Prod. 203. https://doi.org/10.1016/j.jclepro.2018.08.127.

Keshtegar, B., Heddam, S., Kisi, O., Zhu, S.P., 2019. Modeling total dissolved gas (TDG) concentration at Columbia river basin dams: high-order response surface method (H-RSM) vs. M5Tree, LSSVM, and MARS. Arab. J. Geosci. 12. https://doi.org/10.1007/s12517-019-4687-3.

Kokabian, B., Gude, V.G., 2019. Microbial desalination systems for energy and resource recovery. Biomass Biofuels Biochem. Microb. Electrochem. Technol. Sustain. Platf. Fuels, Chem. Remediat. 999–1020. https://doi.org/10.1016/B978-0-444-64052-9.00041-8.

Lu, Y.Y., Hu, Y.D., Zhang, X.L., Wu, L.Y., Liu, Q.Z., 2007. Optimum design of reverse osmosis system under different feed concentration and product specification. J. Memb. Sci. 287. https://doi.org/10.1016/j.memsci.2006.10.037.

Luo, J., Li, M., Hoek, E.M.V., Heng, Y., 2023. Supercomputing and machine learning-aided optimal design of high permeability seawater reverse osmosis membrane systems. Sci. Bull. 68. https://doi.org/10.1016/j.scib.2023.01.039.

Ma, S., Wu, X., Fan, L., Xie, Z., 2024. Predicting water flux and reverse solute flux in forward osmosis processes using artificial neural networks (ANN) modelling with structural parameters. Sep. Purif. Technol. 351, 128092. https://doi.org/10.1016/J.SEPPUR.2024.128092.

Mahadeva, R., Kumar, M., Gupta, V., Manik, G., Patole, S.P., 2023. Modified Whale optimization algorithm based ANN: a novel predictive model for RO desalination plant. Sci. Rep. 13, 1–14. https://doi.org/10.1038/S41598-023-30099-9;SUBJMETA=166,172,639,704;KWRD=ENGINEERING,ENVIRONMENTAL+SCIENCES.

Mehrad, M., Bajolvand, M., Ramezanzadeh, A., Neycharan, J.G., 2020. Developing a new rigorous drilling rate prediction model using a machine learning technique. J. Pet. Sci. Eng. 192. https://doi.org/10.1016/j.petrol.2020.107338.

Mijwil, M.M., 2018. Artificial Neural networks advantages and disadvantages. J. Jar. Syaraf. Tiruan.

Nazif, S., Mirashrafi, E., Roghani, B., Bidhendi, G.N., 2020. Artificial intelligence–Based optimization of Reverse osmosis systems operation performance. J. Environ. Eng. 146, 04019106. https://doi.org/10.1061/(ASCE)EE.1943-7870.0001613/ASSET/7090999D-DA32-4852-A28D-849E72258653/ASSETS/IMAGES/LARGE/FIGURE6.JPG.

Nour-Mohammad, M., Fakhroleslam, M., 2025. Sustainable Reverse osmosis desalination systems: comprehensive superstructure modeling and multi-objective optimization. Ind. Eng. Chem. Res. 64, 6580–6595. https://doi.org/10.1021/ACS.IECR.4C03467/ASSET/IMAGES/LARGE/IE4C03467_0012.JPEG.

Prakash Maran, J., Sivakumar, V., Thirugnanasambandham, K., Sridhar, R., 2013. Artificial neural network and response surface methodology modeling in mass transfer parameters predictions during osmotic dehydration of Carica papaya L. Alexandria Eng. J. 52. https://doi.org/10.1016/j.aej.2013.06.007.

Raju, M., Govindaraju, P.B., Van Duin, A.C.T., Ihme, M., 2018. Atomistic and continuum scale modeling of functionalized graphyne membranes for water desalination. Nanoscale 10. https://doi.org/10.1039/c7nr07963j.

Rakhimbekova, A., Madzhidov, T.I., Nugmanov, R.I., Gimadiev, T.R., Baskin, I.I., Varnek, A., 2020. Comprehensive analysis of applicability domains of QSPR models for chemical reactions. Int. J. Mol. Sci. 21. https://doi.org/10.3390/ijms21155542.

Rall, D., Schweidtmann, A.M., Kruse, M., Evdochenko, E., Mitsos, A., Wessling, M., 2020. Multi-scale membrane process optimization with high-fidelity ion transport models through machine learning. J. Memb. Sci. 608. https://doi.org/10.1016/j.memsci.2020.118208.

Sadri, S., Khoshkhoo, R.H., Ameri, M., 2016. Multi objective optimization of reverse osmosis desalination plant with exergy approach. J. Mech. Sci. Technol. 30, 4807–4814. https://doi.org/10.1007/S12206-016-0953-4/METRICS.

Salehi, K., Daraei, H., Teymouri, P., Maleki, A.: Hydrothermal synthesis of surface-modified copper oxide-doped zinc oxide nanoparticles for degradation of acid black 1: modeling and optimization by response surface methodology. (2014).

Shahid, M.K., Choi, Y., 2022. CO2 as an alternative to traditional antiscalants in pressure-driven membrane processes: an experimental study of lab-scale operation and cleaning strategies. Membranes 12. https://doi.org/10.3390/membranes12100918.

Shokrollahi, A., Tatar, A., Safari, H., 2015. On accurate determination of PVT properties in crude oil systems: committee machine intelligent system modeling approach. J. Taiwan Inst. Chem. Eng. 55. https://doi.org/10.1016/j.jtice.2015.04.009.

Singh, S., Ghosh, S.K., 2022. A unique artificial intelligence approach and mathematical model to accurately evaluate viscosity and density of several nanofluids from experimental data. Colloids Surf. A Physicochem. Eng. Asp. 640. https://doi.org/10.1016/j.colsurfa.2022.128389.

Skuse, C., Gallego-Schmid, A., Azapagic, A., Gorgojo, P.: Can emerging membrane-based desalination technologies replace reverse osmosis?, (2021).

Song, Y., Xie, X., Wang, Y., Yang, S., Ma, W., Wang, P., 2021. Energy consumption prediction method based on LSSVM-PSO model for autonomous underwater gliders. Ocean Eng. 230. https://doi.org/10.1016/j.oceaneng.2021.108982.

Stokes, J.R., Horvath, A., 2009. Energy and air emission effects of water supply. Environ. Sci. Technol. 43, 2680–2687. https://doi.org/10.1021/ES801802H/SUPPL_FILE/ES801802H_SI_001.PDF.

Stover, R.L., 2004. Development of a fourth generation energy recovery device. A CTO Notebook Desalin. 165, 313–321. https://doi.org/10.1016/J.DESAL.2004.06.036.

Talib, N.S.R., Halmi, M.I.E., Ghani, S.S.A., Zaidan, U.H., Shukor, M.Y.A., 2019. Artificial Neural networks (ANNs) and response surface methodology (RSM) approach for modelling the optimization of chromium (VI) reduction by newly isolated Acinetobacter radioresistens strain NS-MIE from agricultural soil. Biomed Res. Int. 2019. https://doi.org/10.1155/2019/5785387.

Tong, T., Elimelech, M.: The global rise of zero liquid discharge for wastewater management: drivers, technologies, and future directions, (2016).

Vince, F., Marechal, F., Aoustin, E., Bréant, P., 2008. Multi-objective optimization of RO desalination plants. Desalination 222. https://doi.org/10.1016/j.desal.2007.02.064.

Voutchkov, N.: Energy use for membrane seawater desalination – current status and trends, (2018).

Voutchkov, N.: Desalination project cost estimating and management. (2018).

Wang, X., Sun, X., Wu, Y., Gao, F., Yang, Y., 2024. Optimizing reverse osmosis desalination from brackish waters: predictive approach employing response surface methodology and artificial neural network models. J. Memb. Sci. 704, 122883. https://doi.org/10.1016/J.MEMSCI.2024.122883.

Wilf, M., Bartels, C., 2005. Optimization of seawater RO systems design. Desalination 173, 1–12. https://doi.org/10.1016/J.DESAL.2004.06.206.

Wu, C., Wang, S., Yuan, J., Li, C., Zhang, Q., 2020. A prediction model of specific productivity index using least square support vector machine method. Adv. Geo. Energy Res. 4. https://doi.org/10.46690/AGER.2020.04.10.

Xue, X., 2017. Prediction of slope stability based on hybrid PSO and LSSVM. J. Comput. Civ. Eng. 31. https://doi.org/10.1061/(asce)cp.1943-5487.0000607.

Zhang, L., Chao, B., Zhang, X., 2020. Modeling and optimization of microbial lipid fermentation from cellulosic ethanol wastewater by Rhodotorula glutinis based on the support vector machine. Bioresour. Technol. 301. https://doi.org/10.1016/j.biortech.2020.122781.

Zhou, L., Wang, B., Jiang, J., Pan, Y., Wang, Q., 2017. Predicting the gas-liquid critical temperature of binary mixtures based on the quantitative structure property relationship. Chemom. Intell. Lab. Syst. 167. https://doi.org/10.1016/j.chemolab.2017.06.009.